PAPER • OPEN ACCESS

Hot electron and ion spectra on blow-off plasma free target in GXII-LFEX direct fast ignition experiment

To cite this article: T. Ozaki *et al* 2023 *Nucl. Fusion* **63** 036009

OPEN ACCESS
IOP Publishing | International Atomic Energy Agency
Nuclear Fusion
Nucl. Fusion **63** (2023) 036009 (8pp)
https://doi.org/10.1088/1741-4326/acb44d

Hot electron and ion spectra on blow-off plasma free target in GXII-LFEX direct fast ignition experiment

T. Ozaki[1,*], Y. Abe[2], Y. Arikawa[2], Y. Sentoku[2], J. Kawanaka[2], S. Tokita[2], N. Miyanaga[2], T. Jitsuno[2], Y. Nakata[2], K. Tsubakimoto[2], A. Sunahara[3], T. Jhozaki[4], E. Miura[5], O. Komeda[6], A. Iwamoto[1], H. Sakagami[1], S. Okihara[7], K. Ishii[7], R. Hanayama[7], Y. Mori[7] and Y. Kitagawa[7]

[1] National Institute for Fusion Science, 322-6 Oroshi/Toki, Gifu 509-5292, Japan
[2] Institute of Laser Engineering, Osaka University, 2-6 Yamada-oka/Suita, Osaka 565-0871, Japan
[3] Purdue University, 610 Purdue Mall, West Lafayette, IN 47907, United States
[4] Hiroshima University, 1-3-2 Kagamiyama/Higashihiroshima, Hiroshima 739-8511, Japan
[5] National Institute of Advanced Industrial Science and Technology, 1-1-1 Umezono/Tsukuba, Ibaraki 305-8560, Japan
[6] Toyota Motor Corporation, 1 Toyota-cho/Toyota, Aichi 471-8571, Japan
[7] The Graduate School for the Creation of New Photonics Industries, 1955-1, Kurematsu-cho, Nishi-ku/Hamamatsu, Shizuoka 431-1202, Japan

E-mail: ozaki@nifs.ac.jp

Received 5 January 2022, revised 14 December 2022
Accepted for publication 18 January 2023
Published 2 February 2023

Abstract

Polystyrene deuteride shell targets with two holes were imploded by the Gekko XII laser and additionally heated by the LFEX laser in a direct fast ignition experiment. In general, when an ultra-intense laser is injected into a blow-off plasma created by the imploding laser, electrons are generated far from the target core and the energies of electrons increase because the electron acceleration distance has been extended. The blow-off plasma moves not only to the vertical direction but to the lateral direction against the target surface. In a shell target with holes, a lower effective electron temperature can be realized by reducing the inflow of the implosion plasma onto the LFEX path, and high coupling efficiency can be expected. The energies of hot electrons and ions absorbed into the target core were calculated from the energy spectra using three electron energy spectrometers and a neutron time-of-flight measurement system, Mandala. The ions have a large contribution of 74% (electron heating of 4.9 J and ion heating of 14.1 J) to target heating in direct fast ignition.

Keywords: LFEX, Gekko XII, shell target with holes, ESM, neutron

(Some figures may appear in colour only in the online journal)

* Author to whom any correspondence should be addressed.

1. Introduction

Fast ignition [1] has been performed by additionally heating an imploded core using an ultra-intense laser. It produces a relativistic electron beam. The core is additionally heated by three mechanisms, electron/ion drag heating, Joule heating by the return current and diffusive heating from the laser-plasma interaction region. Electron/ion drag heating is the most essential mechanism. At an early stage, the heating laser had been injected directly on the imploded core. In general, when an ultra-intense laser is injected into a blow-off plasma, electrons are generated far from the target core and the energies of electrons increase. It was found that dense blow-off plasma disturbed the penetration of the heating laser and sufficient energy coupling efficiency could not be obtained. Therefore, the current mainstream in fast ignition [2, 3] is to attach a cone along the path of the heating laser to prevent the invasion of the blow-off plasma. However, it is difficult to accept a target with a cone in a future fusion reactor because this target is very complicated. For this reason, research into direct fast ignition [4–6] has also been continued.

The hot electron effective temperature ($T_{\rm eff}$) should be maintained lower in order to obtain the high coupling efficiency because the ratio of the deposited energy to the electron energy into the core becomes large at lower $T_{\rm eff}$. Here, the $T_{\rm eff}$, which is evaluated by the slope of the energy spectrum, is equivalent to the average electron energy if the Maxwellian distribution of the electron energy spectrum is assumed. If the laser energy is the same, the lower $T_{\rm eff}$ means that larger numbers of electrons are generated. In order to achieve the lower $T_{\rm eff}$, the pre-formed plasma before the main pulse of the heating laser on the laser path should be suppressed. One of the pre-formed plasmas is the blow-off from the imploding plasma. Another is created by the pre-pulse of the heating laser itself. An electron acceleration takes place around the critical density region in those pre-formed plasmas. If the scale length of the pre-formed plasma is long, the $T_{\rm eff}$ becomes high. The distance between the laser plasma interaction and the core is also important. In general, hot electrons have a divergence angle. When the distance is large, the irradiation efficiency of the electrons against the core decreases.

Direct fast ignition had not been adopted because the blow-off from imploding plasma is unavoidable. However, this problem may be reduced by using a target with holes [7] along the heating laser path. The shell target is cylindrically imploded, and a heating laser is injected at the implosion timing. Since the amount of blow-off plasma is small on the heating laser path, the electron acceleration will be decreased, and the position of the laser plasma interaction can be close to the core. Therefore, high irradiation efficiency can be expected. The holes may be able to reduce pre-pulse of the heating laser. If the main pulse is adjusted to the maximum compression timing of the imploding core, the pre-pulse can pass through the holes and omit the pre-formed plasma by the pre-pulse. Therefore, the laser energy can be effectively injected even by the heating laser with a poor contrast. For those reasons, the shell with holes has the conditions for lower $T_{\rm eff}$.

In direct heating, ion heating cannot be ignored. In an intense laser, the ponderomotive acceleration (and/or Coulomb explosion) and target normal surface acceleration (TNSA)-like, are occurred. We use the expression 'TNSA-like' here because the target surface is covered with plasma (not vacuum). But it can be regarded as TNSA as a whole. Here, we call TNSA 'TNSA-like' because it is accelerated by the sheath electric field created by hot electrons. The ponderomotive acceleration etc seems to contribute to the core heating because many ions are oriented to the laser direction. On the other hand, TNSA-like acceleration is mechanism with the target behind it. Therefore, the contribution of the core heating is considered to be small.

The electron-ion energy spectrometer (ESM) [8] and the Mandala neutron time-of-flight analyzer (Mandala) [9] are used to estimate the deposited energy of electrons and ions, which contribute to the heating. The results are compared with the absorbed energy obtained from areal density (ρR) and x-ray measurement [10]. The details of the diagnostics are explained in section 2.

Here, we focus on the results of transverse irradiation [11] by adding the simulation results. The details of the simulation are explained in section 3.1.

2. Experimental setup

The experiment was performed using the Gekko XII (GXII)-LFEX [12] facility in the Institute of Laser Engineering of Osaka University. The GXII (wavelength of 0.53 μm) and the LFEX (1.054 μm) were used for target implosion and for additional heating, respectively. As a target, spherical shells of deuterium polystyrene, which have a diameter of 500 μm in diameter and a thickness of 7 μm were used. There are two holes of 100 μm in diameter in this target at a position 180° apart. The LFEX is injected along a line connecting the centers of two holes. Cylindrical implosion is performed using six beams (named each as B04, 07, 09, 10, 11 and 12) in 12 beams, which are almost perpendicular in direction against the LFEX beam (transverse irradiation). Figure 1(*a*) (i)/(iii) and (ii)/(iv) show the irradiation arrangement of the GXII seen from the LFEX axis, and the irradiation coordination seen from the side, respectively. Three beams are irradiated to the target at equal intervals, as seen from the LFEX direction. The remaining three beams are irradiated from the counter side of the LFEX. The angle between the GXII and LFEX is 79.2° in the transverse irradiation. The blow-off plasma is sufficiently far from the LFEX axis. Since there are holes on the LFEX axis, the ablation plasma is further reduced.

In the experiment, three different injection timings of the implosion laser and the heating laser were chosen. The energy of the implosion laser was (246–301) J × 6 beams = 1.545–1.738 kJ with 1.1–1.3 ns with Gaussian shape. The LFEX laser consisted of two rectangular beams with 1–1.8 ps, about (202–287) × 2 beams ×60% (irradiation efficiency) = 243–343 J on target. Sixty percent means the efficiency through the optical components after the last monitoring system [13].

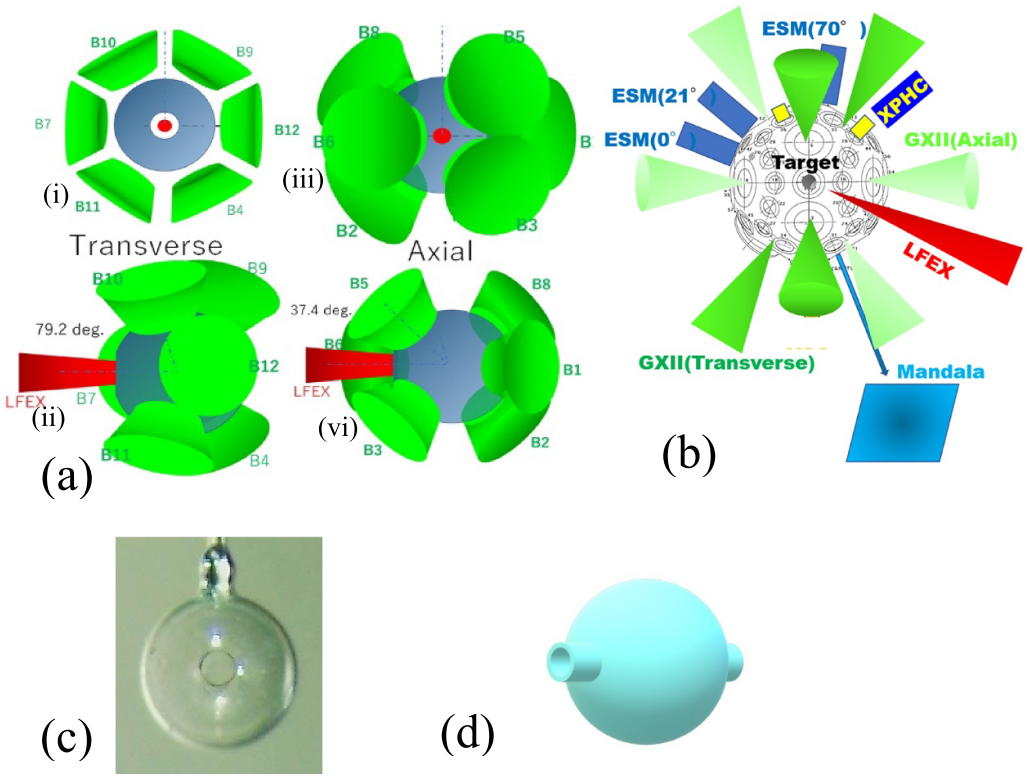

Figure 1. Laser and diagnostics arrangements. (*a*) The GXII (green) and LFEX (red) laser arrangements, The GXII and the LFEX are used for compression and additional heating, respectively. B1, B2, B3 etc (Dark green) means the names of the GXII beams. The GXII is tilted 79.2° with respect to the LFEX for transverse irradiation, and 37.4° for axial irradiation (i) and (ii) show sight and side views from the LFEX axis in transverse irradiation, respectively. (iii) and (iv) show sight and side views from the LFEX axis in axial irradiation, respectively. Polystyrene targets (blue) with and without holes are used in transverse and in axial irradiations, respectively. (*b*) Diagnostics arrangements, Three ESMs are installed at 0 and 21 and 70° against the counter direction of the LFEX. XPHCs are installed at 125 and 70° from the LFEX laser counter direction. The Mandala is located 13.55 m from the target at 125.3° from the LFEX counter direction. (*c*) Photograph of the target. (*d*) Target with fins(ideal).

The focus diameter was estimated to be 50 μm in diameter. The irradiation intensity was over 10^{19} W cm^{-2}, which was in the relativistic region. Therefore, the generation of the energetic electrons and ions could be expected. For comparison, another experiment was also conducted in which the GXII was irradiated in a parallel direction to the LFEX (axial irradiation, B01, 02, 08, 03, 05, 06). The arrangement is shown in figure 1(*a*) (iii) and (iv). The angle between GXII and LFEX is 37.4°. In this arrangement, the ablation plasma invades easily in the cone angle of the LFEX beam. Figures 1(*b*) and (*c*) are the arrangements of the diagnostics and the target, respectively.

The behaviors of hot electrons and ions are measured using the ESM and Mandala. Three ESMs are installed at 0°, 21°, and 70° from the LFEX forward direction. Electrons measured by the ESM are those that can be emitted by shaking off the potential near the target. Electrons with energies below this potential are not observed by the ESM. Therefore, the amount of particles observed by it is much smaller than that of generated particles. The electron energy distribution is observed with the shape unchanged and shifted by the potential. Assuming Maxwell distribution, the $T_{\rm eff}$ will be the average energy if the $T_{\rm eff}$ = the slope of the distribution is known. The installation position is on the chamber 0.89 m from the target. ESMs can measure hot electrons (measurable energy range: 0.5 MeV–120 MeV) and protons (up to 7 MeV) or deuterium ions (up to 3.5 MeV), at the same time, by using a permanent magnet. The ESM has a very low leakage magnetic field because the magnetic circuit is suitably designed. Therefore, a large energy dynamic range can be achieved. Unfortunately, there is no ability to distinguish ion species. However, we can estimate the proton/deuteron ratio roughly by using the aluminum filter method [14].

The Mandala is located on 13.55 m from the target at 125.3° from the LFEX forward direction. The Mandala consists of an array of 600 photomultipliers. The energies of neutrons can be obtained from the flight times. For the DD reaction between the deuterium target and the deuteron beam generated by the LFEX laser acceleration, backscattered neutrons with mainly lower than 2.45 MeV are measured. The advantage of the Mandala is that it can accurately observe the spectrum of neutrons of 10^6, even in a strong gamma ray environment during LFEX operation. In addition, CR-39 was used to measure ρR at implosion shots without the LFEX injection. ρR can be estimated by the energy loss of knock-on protons between the target and thermal DD neutrons. The x-rays come.

3. Experimental results

The energy spectra of electrons and ions can be obtained from ESMs. In the experiment, the GXII irradiates to the target and the LFEX is injected into the core at two different timings. Electron and ion drag heatings are evaluated from their energy spectra and neutron results. Figure 2(*a*) shows the pulse waveform of the GXII and T_{eff}. Figure 2(*b*) shows the soft x-ray generation time history [15] from the imploding plasma obtained by the simulation (STAR2D [16]) and the injection timing of the LFEX. The peak time of soft x-rays seems to be the maximum compression time. A total of three shots were conducted. The LFEX was incident 200 ps before (twice) and 300 ps after the maximum compression time.

3.1. Electron

Figure 3(*a*) shows a comparison of typical electron energy spectra measured in the counter direction of the LFEX for transverse and axial irradiations. The T_{eff} in transverse irradiation is clearly lower than that in axial irradiation because the blow-off from the imploding plasma is smaller in the former than in the latter. In transverse irradiation, it is difficult that the GXII irradiates the shell near the LFEX axis, and there is no ablation plasma because there are holes. Furthermore, the pre-pulse has passed during implosion through the holes in the imploding shell. The LFEX irradiates the core if we can adjust its injection timing to the maximum compression timing. The only wraparound of the explosive plasma from its surroundings blocks the LFEX path in transverse irradiation. Therefore, the T_{eff} remains low in transverse irradiation.

Rough spatial distributions of hot electrons can be obtained from the three ESMs. Comparisons of the spatial distribution of the electron spectra in transverse and axial irradiations have been performed. Figures 3(*b*) and (*c*) show those contour plots. In axial irradiation, electrons with a high T_{eff} at 0° are observed, whereas in transverse irradiation, the T_{eff} remains low at 0°. The low T_{eff} is convenient for fast ignition. It should be noted here that the absolute value of the number of electrons measured by the ESM is not proportional to the number of generated electrons. Since the electrons generated around the target are suppressed by the self-electromagnetic field and do not reach the position of ESM, the number of particles observed by it depends on the T_{eff}. Therefore, we focus more on the spectral shape than on the absolute amount of the signal.

In figure 4, the simulation results of the core plasma behavior at −200 ps and +300 ps are also plotted. Implosion characteristics were investigated using the 2D radiation-hydrodynamic simulation code STAR2D [16, 17] in a cylindrical coordinate. 3D distribution of the laser intensity was averaged around the symmetrical axis, and converted to 2D distribution. The simulation was conducted for a cylindrical geometry. It was originally developed for modeling extreme ultraviolet light source plasmas. We deal with laser-produced plasmas by solving propagation by laser ray-tracing, laser absorption by inverse bremsstrahlung, heat conduction, radiation transport, and temperature relaxation between ions and electrons. The sound velocity is calculated from the equation of state, and the flow velocity is calculated using the fluid solver HLLC (Harten–Lax–van Leer contact wave) [18] method, based on the sound velocity. The radiation transport was solved by a multi-group diffusion model with 40 groups, in which the maximum photon energy was 8 keV. The electron and ion heat conduction were calculated based on the flux limited Spitzer–Harm model [19] with a flux-limiter of 0.1.

The hot electron generation point is the interaction region between the LFEX laser and the ablation plasma. Ideally, the generation point should be close to the core, but according to

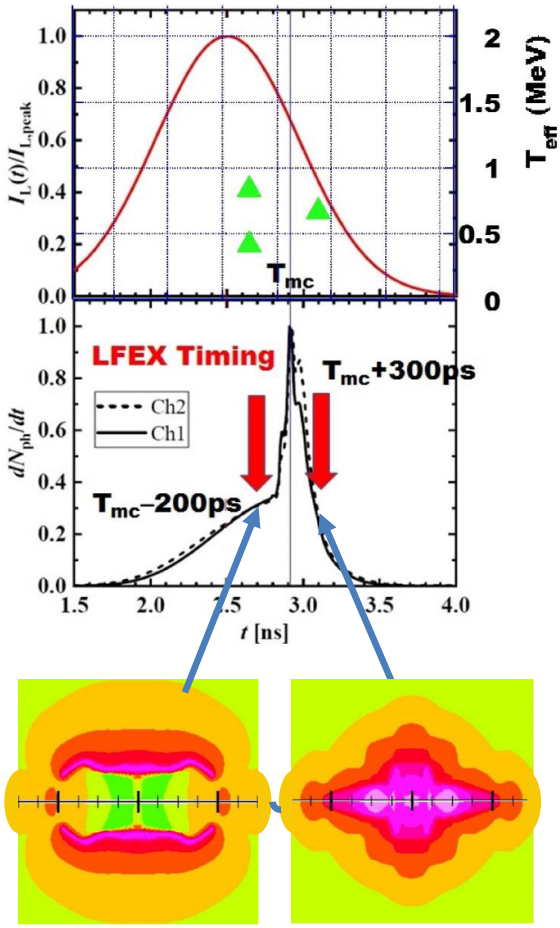

Figure 2. GXII waveform and LFEX injection timing. The intensity waveform of GXII has a Gaussian profile with a pulse width of 1.1–1.3 ns. The beam energy is an average 250 J/beam. T_{eff} is also plotted on the same figure. The LFEX injection timings are also shown in a lower figure. (upper) The GXII waveform and the T_{eff} in a counter direction to the LFEX laser (green triangles). Mainly hard x-rays are generated when hot electrons collide with targets and other structures. Error bars come from the comparison of two different ways of hard x-ray noise reduction. However, error bars are hidden in the symbols because they are within ±0.03 MeV. (lower) x-ray emissions from the core in simulation. The x-rays come from the imploded core. They show a comparison with laser injection timing. Red arrows show the LFEX injection timings. The photon energy range corresponds to an imaging plate (IP) used in the experiment. The signal is the integral of the sensitivity of the IP (400–800 nm). The unit of x-ray emission is the number of photons per second. It is normalized by the peak because an absolute value is not necessary here. T_{mc} means the maximum compression time. The details of the simulation are described in section 3.1.

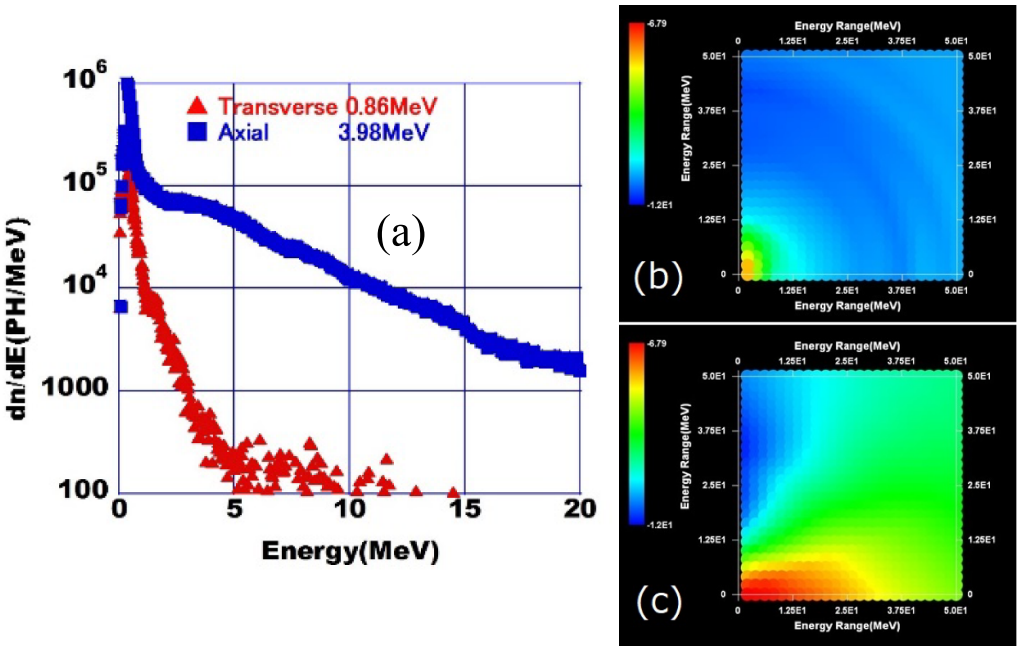

Figure 3. Electron energy spectra. The spectra of hot electrons were compared under transverse and axial irradiation. Transverse irradiation is clearly optimal for fast ignition. An angular contour plot was prepared to express the spatial distribution of the spectrum. It can be seen that the transverse irradiation is almost isotropic. (*a*) Comparison of electron spectra at 0° between in transverse and in axial irradiations. $T_{\rm eff}$s are written on the upper part of the graph, (*b*) contour plot in transverse irradiation, (*c*) contour plot in axial irradiation. In (*b*) and (*c*), it will be the same energy if concentric circles are drawn from the origin since it is a polar coordinate. Rotating the horizontal axis by θ around the origin, the electron energy spectrum at the observation direction θ can be obtained from the imploded core. X-ray pinhole cameras (XPHC) were used to measure the size of the core plasma.

computer simulation, the blow-off plasma partially invades the LFEX path at this timing, even in transverse irradiation. It can be that the electrons of the solid angle Ω, that see the target from the generation point, hit the target. Even the laser intensity is in the relativistic region, and there are primary interaction regions at 220 μm (−200 ps) and 240 μm (+300 ps) from the core center. Ωs are $4\pi \times 0.082$ (−200 ps) and $4\pi \times 0.017$ (+300 ps), respectively. Average $T_{\rm eff}$ ($=T_{\rm eff\_ave}$) in which spatial uniformity is considered, are 1.06 MeV at −200 ps and 1.05 MeV at +300 ps, respectively. The reflection of the LFEX laser has been measured on a variety of targets in other experiment [20]. Many researchers have argued about the efficiency of laser-to-electron conversion. Chen [21] calculated the number of hot electrons passing through the target from the line intensity of $K\alpha$ and estimates the conversion rate to be 20%–40%. Norreys [22] showed that the energy coupling to the forward hot electron beam is in the range of 15%–30%. The discussion here is not far from these results. The reflection mainly depends on laser intensity. The remaining 75% of the 25% of the laser reflection is assumed here to transfer energy to the electrons. Actually some energies are directly transferred to ions (ponderomotive acceleration etc), but they are relatively small. Energies transferred to ions in TNSA and converted to electromagnetic waves such as x-rays are first transferred to electrons, and energies are transferred to ions and x-rays. The initial number of generated hot electrons can be obtained by dividing the un-reflected laser energy $E_{\rm L}$ by the $T_{\rm eff\_ave}$. There is also the energy that goes directly to ions, but we will discuss that in section 3.2. It is estimated that 25% is reflected in this laser intensity region, and the remaining 75% is converted to electrons. The number of electrons, $N_{\rm elec\_total}$, can be estimated by

$$N_{\rm elec\_total} = E_{\rm L} \times 75\% \div T_{\rm eff\_ave}. \quad (1)$$

Here we assume that the momentum is preserved.

$$\begin{aligned}(\text{momentum\_of\_the\_light}) \approx & \int \{{\rm d}N_{\rm elec}(\Omega)/{\rm d}\Omega\}\boldsymbol{p}(\Omega){\rm d}\Omega \\ & + (\text{ion\_contribution}) \\ & + (\text{reflection\_of\_the\_light}), \quad (2)\end{aligned}$$

where $\boldsymbol{p}(\Omega)$ is the momentum vector ($|\boldsymbol{p}(\Omega)| = m_{\rm e}c\sqrt{\{(1 + T_{\rm eff}(\Omega)/m_{\rm e}c^2)^2 - 1\}}$), c is the light velocity, $m_{\rm e}$ is the electron mass, respectively. Ponderomotive accelerated ions remain as the ion contribution in equation (2), although the ion distribution is almost uniform, as mentioned in section 3.2. $N_{\rm elec}(\Omega)$ becomes large in the direction of lower $T_{\rm eff}(\Omega)$. ${\rm d}N_{\rm elec}/{\rm d}\Omega$ is determined as satisfying $N_{\rm elec\_total} = \int \{{\rm d}N_{\rm elec}/{\rm d}\Omega| \, {\rm d}\Omega| \, 4\pi \{{\rm d}N_{\rm elec}/{\rm d}\Omega\}$ are plotted as a function of angle in figure 4.

The deposited energies of electrons to the target are almost the same as the stopping energy, $E_{\rho R}$, for the target's ρR, if the energies are higher than the $E_{\rho R}$. Total deposited electron energy becomes large if the number of electrons becomes large. ρR is 12.2 mg cm^{-2} at the maximum compression by the recoil proton method using CR-39. We assume that the value has not changed significantly before and after the maximum compression. Therefore, the $E_{\rho R}$ is 0.0079 MeV. Bethe's

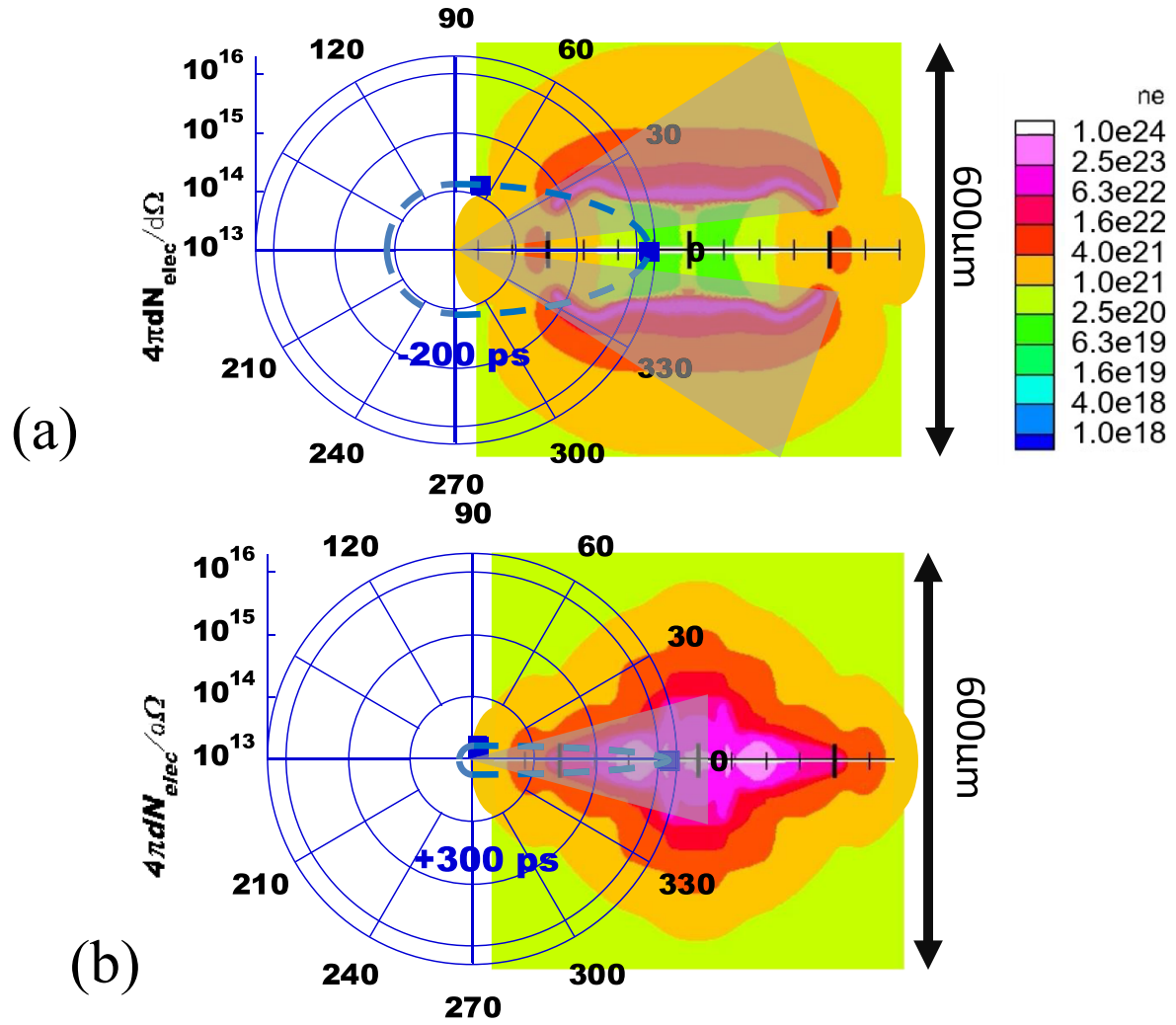

Figure 4. Comparison between simulation (density plot) and ESM results. The color figures show the shape of the target obtained by simulation at the time of LFEX incidence. (*a*) at −200 ps, (*b*) at +300 ps. The electron number distributions in left circular plots are overlapped on the 2D simulation density plots in /cm^3. Broken lines and triangle shadows show the rough electron distribution and the electron trajectory which irradiates the targets. The angular distribution of hot electrons shown by the broken line is obtained as follows. This is the number of electrons per unit solid angle. First, the total number of electrons is obtained by dividing the total energy absorbed by the laser by the average electron energy ($T_{\rm eff}$), the electrons are allocated by the solid angles so that the momentum (originally the momentum brought in by the laser) is preserved.

classical formula is used about the value. Since the energy of the electron is so large, only the energy corresponding to the target, ρR, is lost. ρR is too small in this experiment. The value of the $E_{\rho R}$ is almost same if the electron energy is large compared to the range of ρR. The viewing areas $\omega/4\pi$ from the electron emission region are estimated to be 0.082 (−200 s) and 0.017 (+300 ps), respectively (figure 4). The total electron number which irradiates the target $N_{\rm elec\_target}$ is $\{{\rm d}N_{\rm elec}/{\rm d}\Omega{\rm l} \times \omega$. Therefore, total electron drag is $E_{\rho R} \times N_{\rm elec\_target}$ are 4.9 J and 2.2 J at −200 ps and +300 ps, respectively.

3.2. Ions

The advantage of direct fast ignition is that the ions can be used for heating. Ion acceleration consists of ponderomotive acceleration etc [23]. and the TNSA-like type. These ions mainly contain deuterons and protons. Proton sources are water molecules adsorbed on the surface of the target. The ESM cannot distinguish particle species. Ponderomotive acceleration etc is the main contributor to heating, but it is difficult to distinguish them by the ESM. Figure 5(*a*) shows typical ion spectra. Figure 5(*b*) shows the contour plot of the ion spatial distribution. It can be seen that they are relatively isotropic. At early implosion time, holes of the shell are not completely closed yet. Also, even if the LFEX is injected at a late time of implosion, some ponderomotive accelerated ions can be observed by the ESM at 0° because of an ion path through the gap of ablation plasma. However, the ion distribution seems to be uniform. Here we assume that the energy spectra of ponderomotive accelerated ions and TNSA-like ions are the same. Since the ion

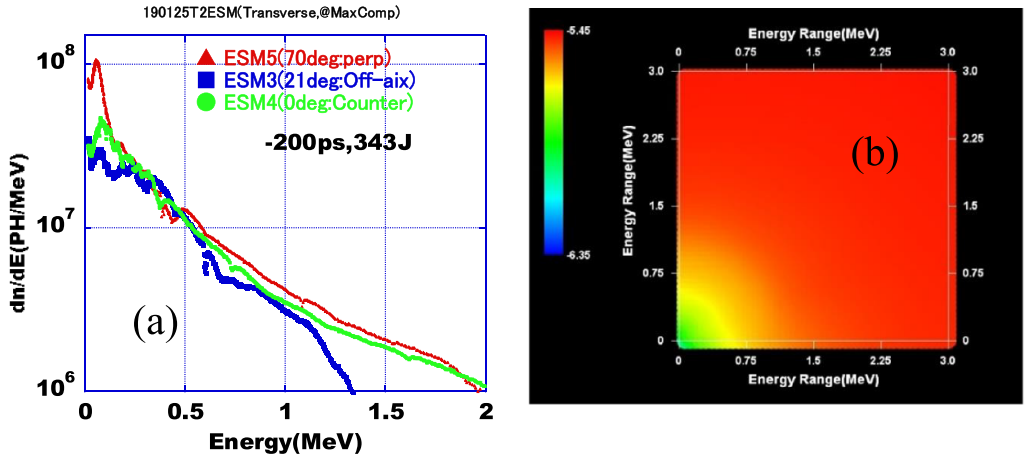

Figure 5. Ion energy spectra. It can be seen that the ion spectrum in transverse irradiation is nearly isotropic. (*a*) Ion spectra, (*b*) contour plot. It is a polar coordinate (contour) of the integrated energy of ions dissipated from the target (mainly TNSA). The *z*-axis (color) is a logarithmic scale. Since it is a polar coordinate, it will be the same energy if concentric circles are drawn from the origin.

stopping range is short, it is assumed that each ion that collides with the high-density part of the target core gives all the energy.

The deposited energy of the ion heating can be estimated from neutron measurement. In nuclear fusion, it is generally produced by a thermonuclear reaction. However, in this experiment, beam fusion neutrons are overwhelmingly larger than thermonuclear neutrons. Here we consider ponderomotive acceleration etc and TNSA as deuterium acceleration mechanisms. If deuterium is accelerated, it will hit the target deuterium and neutrons will be observed. Since TNSA is not oriented in the direction of the target, it is not a contribution of neutron generation because deuterium ions accelerated by TNSA do not collide with the deuteron in the target. Also, thermal neutrons are relatively small in proportion, so they are ignored here. The ponderomotive acceleration etc is the main acceleration mechanism for deuterium (related to neutron generation). Ponderomotive acceleration etc and TNSA assume that the deuterium ratio is the same here. From other experiments [14], the proportion of deuterium among the ions is about 80%, and the rest is primarily protons. Therefore, for ion heating, the value obtained from the neutron measurement caused by deuterium ions may be divided by 0.8. The amount of neutrons, N_y, is larger before the maximum compression than after it [23]. Other neutron sources such as $C(d,n)$, photo nuclear (γ,n) and (p,n) etc can be negligible.

The number of D beams N_{Dbeam} is estimated by,

$$N_{\mathrm{Dbeam}} = N_y / \{\sigma_{\mathrm{DD}} \times N_{\mathrm{D}} \times l_{\mathrm{Range}}\} \propto 1/\{\rho \times l_{\mathrm{Range}}\}, \quad (3)$$

where σ_{DD}, N_{D}, ρ and l_{Range} are the DD nuclear reaction cross-section, the number density of the deuterons in the target, the mass density, and the stopping range, respectively. The mass density at the maximum implosion time ρ_{max} can be estimated from $\rho_{\mathrm{max}}R_{\mathrm{max}}$, obtained by the CR-39 knock-on proton method and R_{max} obtained from the XPHC. Its value is 1.9 g cm^{-3}. The target radius R and ρ at -200 ps, are larger than R_{max} and smaller than ρ_{max} because the implosion is still continued, as shown in figure 3. ρ at -200 ps is estimated to be 1.67 g cm^{-3}. However, the product of ρ and l_{Range} in equation (3) at -200 ps is only 5% different from that at the maximum implosion time. Therefore, $\rho_{\mathrm{max}}R_{\mathrm{max}}$ is adopted as ρl_{Range} at $+300$ ps because it is difficult to evaluate ρl_{Range} at $+300$ ps. The average energy of the ions, T_{ion}, can be estimated to be 0.46 MeV (-200 ps) and 0.33 MeV ($+300$ ps) by approximating the Maxwell distribution of the ion spectrum in figure 4(*a*). l_{Range} at T_{ion} can be calculated by using the SRIM [24] code (solid) and the range difference of 0.6 between solid and hot plasma. ls are 2.25 μm (-200 ps) and 1.38 μm ($+300$ ps).

σ_{DD} at T_{ion} can be obtained to be 0.1 b (-200 ps) and 0.076 b ($+300$ ps). On the other hand, Ny are 2.47×10^8 (-200 ps) and 0.268×10^8 ($+300$ ps) from the Mandala [25]. N_{Dbeam} can be calculated from equation (3). Since l_{Range} is too short compared to the target size, it is assumed that all the ion energies are deposited on the target. As the ratio of deuterium is 80% of the total ions, the number of all ions that irradiate the target can be calculated. Finally, the deposit energy $N_{\mathrm{Dbeam}} \times T_{\mathrm{ion}} \div 0.8$, can be estimated to be 14.1 J (-200 ps) and 1.2 J ($+$ 300 ps).

In this experiment, the injection timing of the LFEX was slightly early compared to the implosion timing, so that the ions were irradiated to a large target viewing angle, although the ion generation point was far from the core. Therefore, considerable neutrons were observed before the implosion than afterwards. It is important to increase the solid angle of irradiation by preventing the blow-off plasma and adjusting to the implosion timing.

4. Discussions

The deposited energy by additional heating was evaluated from the ESM results for transverse irradiation. The T_{eff} is kept sufficiently low, and the difference between the three T_{eff} is simply proportional to the incident energy (intensity). In section 3, the energy added by the LFEX energy of 343 J could

Table 1. Electron heating.

Config.	Shot(19*)	Delay(ps)	E_{L}(J)	$T_{\mathrm{eff\_avg}}$(MeV)	$\omega/4\pi$	$E_{\rho R}$(MeV)	$N_{\mathrm{elec}}(10^{15})$	E_{drag}(J)
Trans.	0125T2	−200	343	1.05	0.082	0.079	1.53	4.9
Trans.	0125T5	+300	309	1.06	0.017	0.079	1.37	2.2
Axial	0124T3	+200	262	2.06	0.413	0.096	0.60	2.3

Table 2. Ion heating.

Config.	Shot(19*)	ρR(g/cm^2)	$l_{\mathrm{Range}}(\mu$m)	ρ(g/cm^3)	N_{Dbeam}	T_{ion}(MeV)	σ_{DD}(b)	$N_{\mathrm{y}}/10^8$	E_{drag}(J)
Trans.	0125T2	0.0122	2.25	1.67	11.5×10^{13}	0.46	0.10	2.47	14.1
Trans.	0125T5	0.0122	1.38	1.90	1.64	0.33	0.076	0.268	1.2
Axial	0124T3	0.0160	1.28	2.86	2.35	0.44	0.107	0.397	2.0

be estimated to be 4.9 J for electrons and 14.1 J for ions. The ions have a large contribution against target heating in direct fast ignition. The results of the electron and ion heatings are listed in tables 1 and 2, respectively.

The electron and ion drags can be also estimated to be 2.3 J and 2.0 J by the same procedure in axial irradiation, respectively; then total amount is 4.3 J. On the other hand, we could succeed in estimating the increment of the internal energy of 3.4 J by using an optical technique in axial irradiation [26]. Those values are closed from each other.

If the internal energy of implosion without additional heating is to be 68 J, the same as that in axial irradiation and the increase of the internal energy is 19.1 J in transverse irradiation, the magnification of the internal energy is 1.28 times. Assuming that the ion temperature before the additional heating is 0.85 keV, the same as that in axial irradiation, it becomes 1.09 keV, which increases the nuclear reaction rate 4.1 times. However, since the amount of neutrons without additional heating is 3.47×10^6, it becomes only 1.44×10^7 by additional heating. Therefore, the thermal neutron signal could not be observed because it was hidden behind the beam neutron signal (2.47×10^8).

5. Summary

In order to increase the efficiency of the additional heat, it is important to close the laser plasma interaction region to the imploded core. According to the simulation, considerable blow-off plasma still invades to the LFEX path, even if in transverse irradiation. If we put a fin around the hole (see figure 1(*d*)), the invasion of the blow-off can be suppressed considerably. According to another simulation, which imitates the configuration without invasion of the blow-off plasma, the laser plasma interaction region can be approached up to 110 μm from the center of the core. As a result, the solid angle of irradiation can be improved to be $4\pi \times 0.5$, and a heating efficiency of 2.3 times can be expected, even if at current low ρR. Attaching the fin around the hole is simpler than attaching a conventional cone, and is realistic for a future fusion reactor.

Acknowledgments

This work is supported by NIFS14KUGK120, KUGK129, NIFS-URSX302, URSX305, IIHH001 and The Graduate School for the Creation of New Photonics Industries.

ORCID iDs

A. Sunahara https://orcid.org/0000-0001-7543-5226
T. Jhozaki https://orcid.org/0000-0002-5738-4661
Y. Mori https://orcid.org/0000-0001-7754-9171

References

[1] Tabak M. *et al* 1626 *Phys Plasmas* **1** 1994
[2] Kodama R. *et al* 2002 *Nature* **418** 933
[3] Sakata S. *et al* 2018 *Nat. Commun.* **9** 3937
[4] Kitagawa Y. *et al* 2005 *Phys. Rev.* E **71** 016403
[5] Kitagawa Y. *et al* 2011 *Plasma Fusion Res.* **6** 1306006
[6] Kitagawa Y. *et al* 2015 *Phys. Rev. Lett.* **114** 195002
[7] Ozaki T. *et al* 2014 *Phys. Scr.* **2014** 014025
[8] Ozaki T., Veshchev E., Ido T., Shimizu A., Goncharov P. and Sudo S. 2012 *Rev. Sci. Instrum.* **83** 10D920–1
[9] Abe Y. *et al* 2018 *Rev. Sci. Instrum.* **89** 110I114
[10] Miura E. *et al* 2020 *High Energy Density Phys.* **36** 100890
[11] Ozaki T. *et al* 2021 *Plasma Fusion Res.* **16** 2404076
[12] Shiraga H. *et al* 2011 *Plasma Phys. Control. Fusion* **53** 124029
[13] Arikawa Y. private communication
[14] Ozaki T. *et al* 2022 *Plasma Fusion Res.* **17** 2404084
[15] Jhozaki T. private communication
[16] Sunahara A. *et al* 2016 *J. Phys.* **717** 012055
[17] Sunahara A., Nishihara K. and Sasaki A. 2008 *Plasma Fusion Res.* **3** 043
[18] Gurski K.F. 2004 *SIAM J. Sci. Comput.* **25** 2165
[19] Malone R.C., McCrory R.L. and Morse R.L. 1975 *Phys. Rev. Lett.* **34** 721
[20] Ozaki T. *et al* 2016 *J. Phys.* **717** 012043
[21] Chen C.D. *et al* 2009 *Phys. Plasma* **16** 082705
[22] Norreys P.A. *et al* 2009 *Nucl. Fusion* **49** 104023
[23] Bulgakova N.M., Stoian R., Rosenfeld A., Hertel I.V., Marine W. and Campbell E.E.B. 2005 *Appl. Phys.* A **81** 345
[24] Ziegler J. F. Interactions Of Ions With Matter (available at: www.srim.org/)
[25] Abe Y. *et al* 2020 *High Energy Density Phys.* **36** 100803
[26] Kitagawa Y. *et al* 2021 *Rev. Laser Eng.* **49** 149 (in Japanese)